

Proceeding Paper

Novel Immobilized Titanium Dioxide onto Peanut Shell-Based Activated Carbon for Advance Oxidation Process Coupled with Response Surface Models in Organic Wastewater Treatment [†]

Kingsley Safo ^{1,*}, Mavis Berko ² and Hillarus Dela Gohoho ³

¹ Department of Chemical and Petrochemicals Engineering, Egypt-Japan University of Science and Technology, New Borg Al-Arab City 21934, Egypt

² School of Nursing and Midwifery, Family Health University College, Teshie-Accra P.O Box TS 669, Ghana; mavisberko5@gmail.com

³ Department of Chemical and Biomolecular Engineering, University of Nebraska, Lincoln, NE 68588-0619, USA; gohoho.dela@ejust.edu.eg

* Correspondence: kingsley.safo@ejust.edu.eg

[†] Presented at the 2nd International Electronic Conference on Processes: Process Engineering—Current State and Future Trends (ECP 2023), 17–31 May 2023; Available online: <https://ecp2023.sciforum.net/>.

Abstract: This work focuses on how to best degrade organic pollutants from wastewater by immobilizing TiO₂ on activated carbon peanut shells (ACPNS) using the co-precipitation method in a hydrothermal process under simulated solar light for the first time. The produced ACPNS–TiO₂ shows a high degradation efficiency of MB dye molecules under a response surface optimization model. The degradation efficiency of the 5th repeated cycle of the ACPNS–TiO₂ was 74.64%, indicating good reusability of the material. This work showed that ACPNS–TiO₂ might be effectively used for industrial wastewater treatment reducing the overall cost of pure chemicals.

Keywords: activated carbon; TiO₂; response surface models; advance oxidation process; optimization analysis



Citation: Safo, K.; Berko, M.; Gohoho, H.D. Novel Immobilized Titanium Dioxide onto Peanut Shell-Based Activated Carbon for Advance Oxidation Process Coupled with Response Surface Models in Organic Wastewater Treatment. *Eng. Proc.* **2023**, *37*, 96. <https://doi.org/10.3390/ECP2023-14681>

Academic Editor: Chi-Fai Chau

Published: 17 May 2023



Copyright: © 2023 by the authors. Licensee MDPI, Basel, Switzerland. This article is an open access article distributed under the terms and conditions of the Creative Commons Attribution (CC BY) license (<https://creativecommons.org/licenses/by/4.0/>).

1. Introduction

Water contamination is a problem faced by many countries today and has affected the entire world due to using this contaminated water for various activities [1]. Water contamination worldwide results from organic, inorganic, and biological pollutants [2]. These pollutants contain toxic chemicals that affect human health and the environment at large. Many methods have been employed in the treatment of this contaminated water, including the convective treatment method and the advance oxidation method [3]. TiO₂-based photodegradation is an advanced oxidation method used to break down these organic contaminants in wastewater, making it safe for use. TiO₂ acts as a photocatalyst that absorbs photons in the presence of ultraviolet radiation to undergo oxidation and reduction reactions to break down the organic contaminant in water [3].

It has strong aqueous stability and photocatalytic activity, making it an ideal catalyst for enhanced photodegradation of water pollutants [2]. Earlier research has shown that using TiO₂ in its powder form leads to high photodegradation efficiency under UV light. It does, however, suffer from a high rate of photogenerated electron/hole recombination, as well as technical difficulties associated with post-treatment of treated water, such as catalyst recycling and achieving powder-free water [4].

Several efforts have been made to improve the photocatalytic activity and the separation of treated effluent by loading the TiO₂ nanoparticles on various supports [5]. TiO₂ coating surfaces have poor photocatalytic performance due to restricted mass transfer of contaminant to the photocatalyst and reduced particle distribution [6]. Supporting the semiconductor on an adsorbent surface, such as activated carbon (AC), has been proven by a

number of studies to make separation from the effluent more easier and more efficient [7,8]. Nevertheless, the cost of pure activated carbon is high, and activated carbon (AC) itself has not been attributed to any photocatalytic properties. It does enhance the adsorption of pollutant molecules on photocatalyst surface, hence boosting the photocatalytic degradation performance [9]. In addition, there are problems with waste disposal that arise before, during, and after industrial and agricultural processing [10]. Several developing nations have poor waste management systems and generate enormous volumes of this kind of trash [10,11]. Inadequate action to mitigate the resultant dangers might have disastrous consequences. Users of water and aquatic life may be placed in danger if these pollutants are washed into water sources [11,12]. Yet, agricultural solid wastes are rich in carbon and might be used as a low-cost and easily accessible carbon adsorbent alternative.

For the first time, agriculture waste (peanut shell) was converted into activated carbon using the top-down approach, and immobilization of TiO₂ nanoparticles was achieved at a mass ratio of 1:3. The novel materials were applied under a simulated solar photo reactor for photodegradation of methylene blue (MB) dye. The impacts of operational factors such as catalyst dosage, pH, and MB concentration were investigated in response surface models. The reusability was assessed based on the optimal parameters, and the operational cost was estimated.

2. Materials and Methods

In this investigation, the peanut shell was obtained from Alexandria, Egypt. Potassium hydroxide (KOH) and sodium hydroxide pellet (99% NaOH) were supplied from Germany (Merck KGaA). Hydrochloric acid (37% HCl), titanium oxide (TiO₂), and methylene blue (99% MB) were obtained from Fisher Scientific Company, Leicester, UK.

The collected peanut shell was washed and dried in an oven at 90 °C for 2 days, after which it was milled to obtain a size of 106 µm. The sample was carbonized at 500 °C for 120 min under an N₂ environment, from which it was soaked overnight in a KOH solution. The sample was then decanted and activated at 900 °C for 120 min under an N₂ environment. The resulting sample was washed until the pH was neutral, dried in an oven for 12 h, and named activated carbon peanut shell (ACPNS). The ACPNS–TiO₂ was prepared by using the co-precipitation approach in a hydrothermal process [13]. In brief, 40 mL of deionized water was combined with 2 g of TiO₂ and 6 g of ACPNS and sonicated for 60 min at 45 kHz. The ACPNS–TiO₂ composite was dried repeatedly at 100 °C overnight. The sample was washed, filtered, and dried at 110 °C for 60 min to remove any surplus impurities. The resulting sample was then calcinated for another 60 min at 600 °C and named immobilized ACPNS–TiO₂.

The composition of the produced samples, including the chemical and elemental components, was determined using Energy-Dispersive X-ray Spectroscopy (JEOL JEM-2100F, JEOL Ltd., Kyoto, Japan) and X-Ray fluorescence (Shimadzu XRF, Shimadzu Corporation, Kyoto, Japan). A scanning electron microscope was used to examine the microstructure, morphology, and nanostructure of the prepared sample (JEOL JSM-6010LV SEM, JEOL Ltd.). High-resolution images were obtained using a transmission electron microscope (TEM). The samples' bonds and functional groups were also investigated using a Fourier Transform Infrared Spectrometer (Shimadzu FTIR-8400s, Shimadzu Corporation). X-ray diffraction (Shimadzu XRD-6100, Shimadzu Corporation) with a 1.54 Cu-K radiation beam was used to study the crystallographic structures of novel materials.

The experiment was carried out using the matrix parameters from the response surface models at ACPNS–TiO₂ dosage (10–60 mg/L), pH (2–12), and MB concentrations of 10–50 ppm in a simulated solar photo reactor consisting of a metal halide lamp (Philips) with a photo flux of 220 Wcm², a wavelength of 510 nm, and a power of 400 W placed 15 cm above the solution surface. A total 5 mL of the product was collected in a test tube at 10 min intervals and centrifuged at 6000 rpm for 10 min to remove the nanocomposite

catalyst. MB absorbance was measured using a UV–vis spectrophotometer at a wavelength of 663 nm. The degradation efficiency (η) is then calculated using Equation (1) [14].

$$\eta = (\Delta C)/C_0 \times 100 \quad (1)$$

where C_0 denotes the concentration at zero time, and ΔC denotes the difference between the initial concentration and the concentration at any given time, t . The degradation intermediates and transformation product were identified using liquid chromatography–mass spectrometry (LC-MS (2020), Shimadzu) with the result shown in Figures S1 and S2 displaying complete degradation without toxicity.

3. Result and Discussion

3.1. Characterization of the Prepared Samples

Figure 1a,b show SEM images of the nanocomposite ACPNS and ACPNS–TiO₂. This was conducted to examine the surface morphology of the prepared ACPNS absorbent and ACPNS–TiO₂ photocatalyst. As shown in Figure 1a, at 5000 magnifications, the findings indicate that the ACPNS has a smooth surface with different pore structures. The macropores are wide and connected grains may also be seen in the SEM image. The SEM image of ACPNS–TiO₂ indicates that the spheric nanostructures of the TiO₂ nanoparticles were completely immobilized in the pores of the ACPNS as shown in Figure 1b. The TEM image shown in Figure 1d demonstrates that the immobilization was completed in a nanoforn, and the EdX analysis of the ACPNS–TiO₂ as shown in Figure 1c reveals that prepared catalyst contains 58.03 wt% of C, 14.29 wt% of O, and 27.67 wt% of Ti.

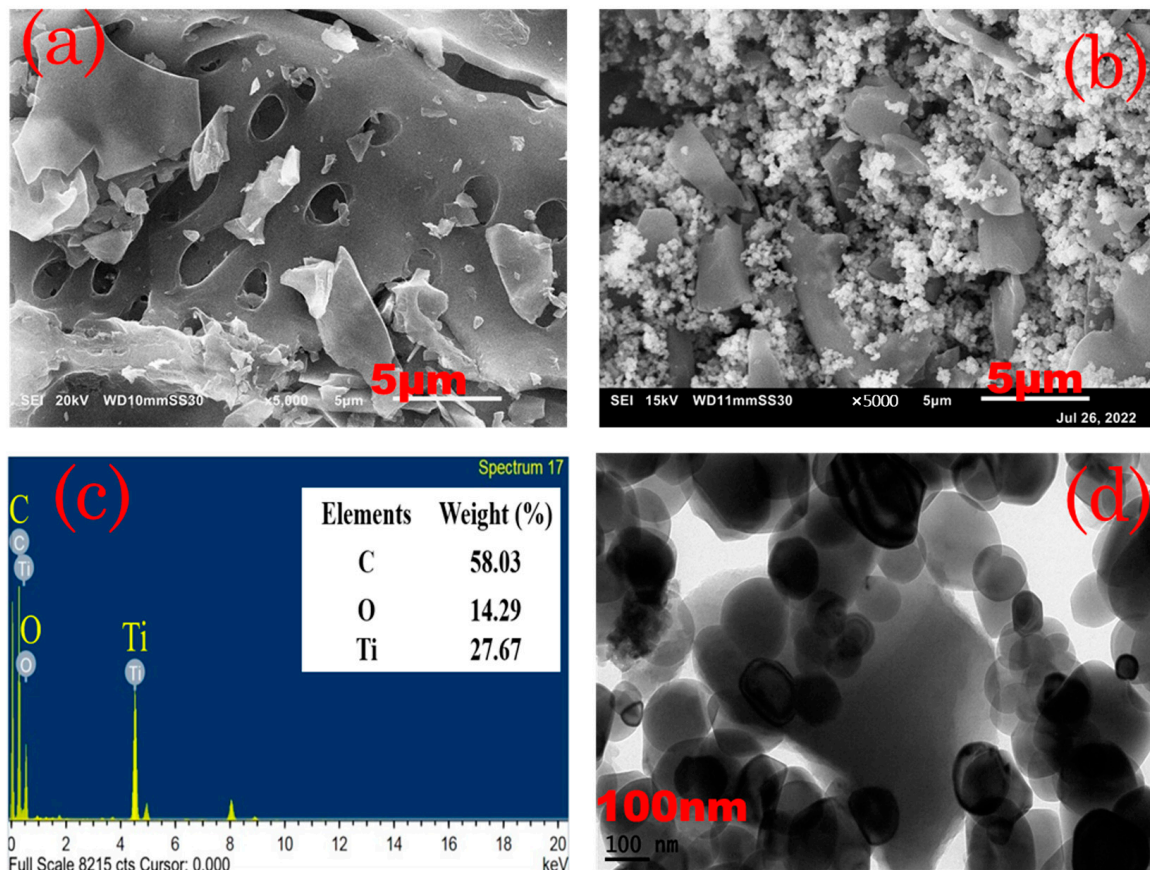


Figure 1. Cont.

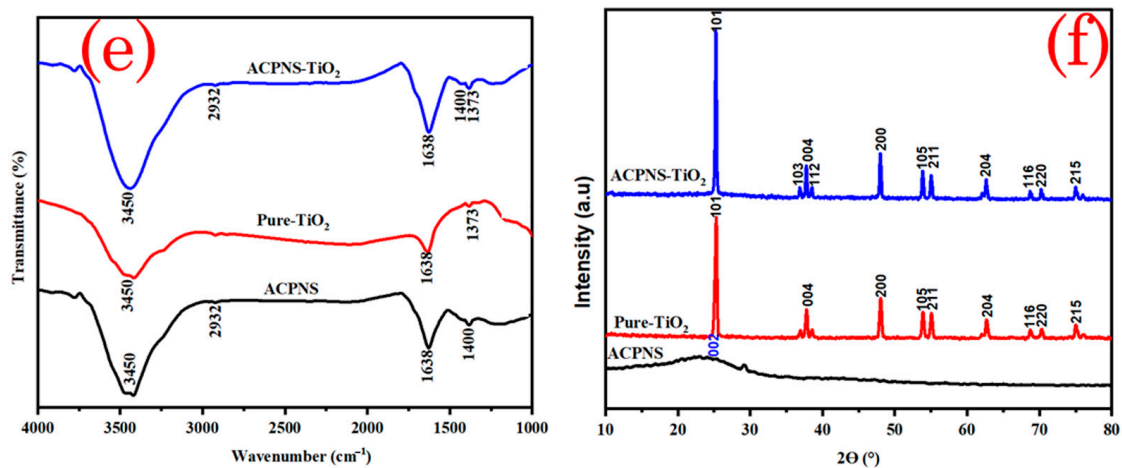


Figure 1. (a) SEM image of ACPNS, (b) SEM image of ACPNS–TiO₂, (c) EDX of ACPNS–TiO₂, (d) TEM of ACPNS–TiO₂, (e) FTIR of ACPNS, Pure TiO₂, and ACPNS–TiO₂ (f) XRD of ACPNS, Pure TiO₂, and ACPNS–TiO₂.

The FTIR spectra in Figure 1e confirm the presence of various functional groups in the crystal lattice, with the stretching vibration bond at 3540 indicating the O–H hydroxy group and that of 2932 showing the C–H vibration in the raw ACPNS and the immobilized ACPNS–TiO₂ [11]. The bending vibration bond at 1638 demonstrates the C=C and O–H bond in the activated carbon, and the TiO₂ with the vibration at 1373 showing the Ti–O bond FTIR spectra stretch bond at 1400 confirms the presence of C–O and C=O bond, which contributes to the absorption of molecules of pollutant [11]. Figure 1f depicts the XRD diffractograms of arbitrarily oriented graphitic microcrystals, as indicated by the peak at $2\theta \approx 26^\circ$, which corresponds to the (002) plane, which is extremely dominant in the ACPNS [11]. The characteristic peaks at 25.31° , 36.95° , 37.80° , 38.57° , 48.03° , 53.89° , 55.07° , 62.69° , 68.72° , 70.30° , and 75.02° correspond to the (101), (103), (004), (112), (200), (105), (211), (204), (116), (220), and (215) crystallographic plane for pure TiO₂, (Anatase, TiO₂ JCPDS Card No. 01-071-1166). The distinctive peaks for pure TiO₂, and ACPNS exist in ACPNS–TiO₂ as shown in Figure 1f, indicating the formation of immobilized ACPNS–TiO₂ at a ratio of 3:1.

3.2. Application of the Produce Novel Catalyst for MB Photodegradation Using Response Surface Models

Seventeen separate experiments were run, and the photodegradation efficiencies of MB dyes were obtained and modeled at 60 min irradiation time using the Box–Behnken design (BBD) model. The link between the factors and the degradation efficiencies of MB is described in Equation (2).

$$Y(\%) = 79.71 + 11.60A + 13.18B - 10.56C - 0.13AB - 2.78AC - 2.72BC - 4.76A^2 - 8.70B^2 - 10.17C^2 \quad (2)$$

where Y (%) is the degradation Efficiency (%) of MB, A is ACPNS–TiO₂ dosage, B is pH, and C is MB Concentration at a time of 60 min. The high value of R² (0.9906) and adjusted R² (0.978) and the standard deviation of 2.43 provided evidence that the model was suitable for the application.

In order to determine whether the model is significant, an ANOVA test for MB degradation efficiency was carried out, and the results are shown in Table 1. According to the F-values and p-values, the ACPNS–TiO₂ dosage and the pH had a more substantial impact on the photodegradation efficiency of MB, while MB concentration had the least amount of influence. Moreover, the low p-value indicates the significance of the prediction model.

Table 1. ANOVA report for the degradation efficiency of MB at 60 min.

Source	Sum of Squares	df	Mean Square	F-Value	p-Value
Model	4356.71	9	484.08	81.81	<0.0001
A-ACPNS–TiO ₂ dosage	1075.55	1	1075.55	181.76	<0.0001
B-pH	1389.96	1	1389.96	234.89	<0.0001
C-MB Concentration	891.90	1	891.90	150.72	<0.0001
AB	0.0676	1	0.0676	0.0114	0.9179
AC	30.91	1	30.91	5.22	0.0562
BC	29.65	1	29.65	5.01	0.0602
A ²	95.51	1	95.51	16.14	0.0051
B ²	318.71	1	318.71	53.86	0.0002
C ²	435.51	1	435.51	73.60	<0.0001
Residual	41.42	7	5.92		
Lack of Fit	35.23	3	11.74	7.59	0.0
Pure Error	6.19	4	1.55		

3.3. Effect of ACPNS–TiO₂ Dosage, pH, and MB Concentration on Degradation Efficiency

The influence of ACPNS–TiO₂ dosage on MB photodegradation efficiency was shown by a 3D response surface plot in Figure 2. The increase in ACPNS–TiO₂ dosage improves MB photodegradation efficiency by increasing the number of active sites that may absorb photons and create reactive species [3,4]. However, applying a catalyst dosage greater than the optimal (56.75 mg/L) reduces the effectiveness of the photodegradation owing to the scattering effect, as shown in Figure 2a. This is because of the increase in solution turbidity, which is caused by the high catalyst dosage leading to the reduction of photons of light exciting the active sites of the catalyst [3,4]. Nevertheless, a positive relationship existed between the ACPNS–TiO₂ dosage and the pH. The reaction interaction effect between ACPNS–TiO₂ dosage and MB concentration can be further described according to the analysis of variance in Table 1. There was a significant relationship between ACPNS–TiO₂ and MB concentration. This relationship is also depicted in the 3D surface plot Figure 2b, where increasing ACPNS–TiO₂ dosage increases degradation efficiency as MB concentration increases. A numerical optimization study was conducted where the optimum operating values were pH of 11.9, ACPNS–TiO₂ dosage of 56.75 mg/L, MB concentration of 20.77 ppm, and an irradiation time of 60 min with photodegradation efficiency of 96.34%.

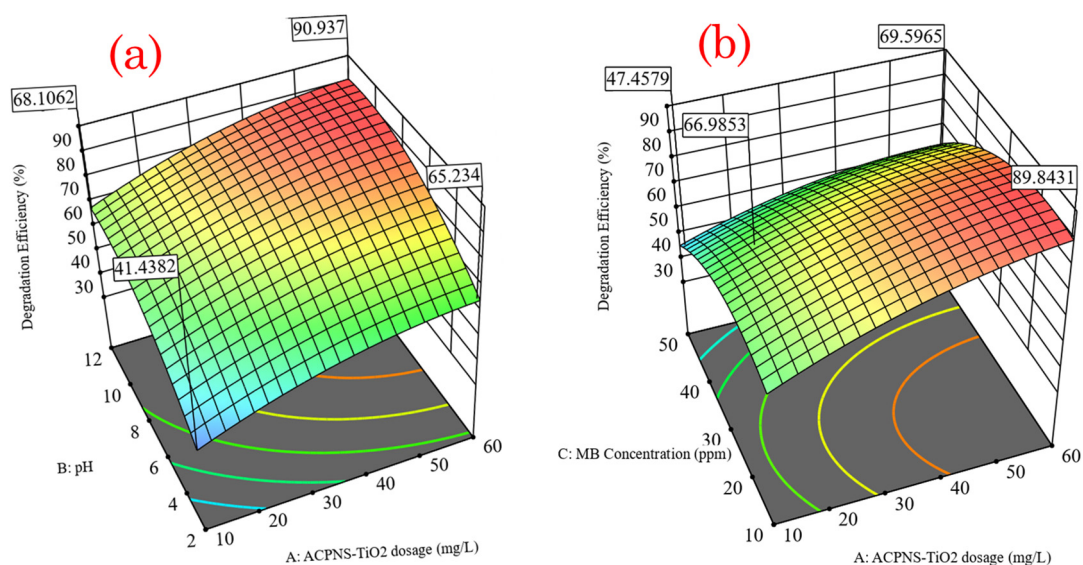


Figure 2. 3D response surface plot of (a) ACPNS–TiO₂ dosage and pH (b) MB concentration and ACPNS–TiO₂ effect on MB dye at irradiation time of 60 min.

3.4. Stability and Reusability of ACPNS–TiO₂

The photodegradation efficiency of MB utilizing immobilized ACPNS–TiO₂ was examined, as demonstrated in Figure 3, in five consecutive repeating cycles of the degradation process at the obtained optimum conditions to evaluate the reusability and industrial application of the ACPNS–TiO₂. The photodegradation efficiencies of the repeating cycle were 96.98%, 94.56%, 85.45%, 81.76%, and 74.64%, respectively, which confirms the stability and reusability of the ACPNS–TiO₂.

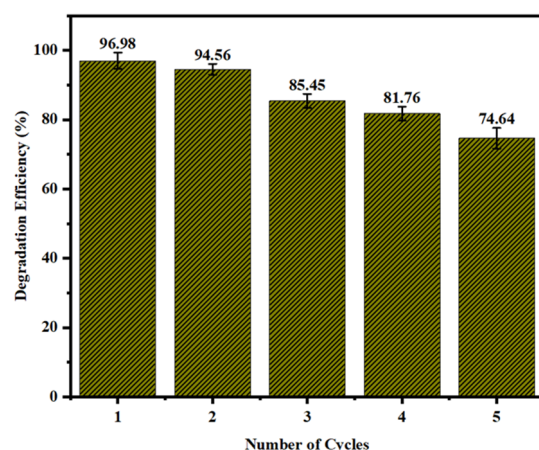


Figure 3. The reusability performance of ACPNS–TiO₂ (conditions: ACPNS–TiO₂ of 56.75 mg/L, pH of 11.9, and MB concentration of 20.77 ppm at irradiation time of 60 min).

4. Conclusions

In this work, raw agriculture waste was successfully synthesized, activated, and TiO₂-immobilized for photodegradation of MB dye. Characterization of the produced materials was achieved for SEM, FTIR, TEM, EDX, and XRD. The result demonstrated that the produced catalyst is in a nanoform with stable immobilization structures composed of different crystalline peaks. The degradation efficiency of ACPNS–TiO₂ was studied, and we achieved almost a complete degradation of MB molecules after 60 min irradiation time. The photodegradation was optimized using response surface models where we attained 96.34% degradation efficiency at a pH of 11.9, ACPNS–TiO₂ dosage of 56.75 mg/L, MB concentration of 20.77 ppm, and a time of 60 min. The MB degradation efficiency in five repeating cycles at the optimum parameters was 96.98%, 94.56%, 85.45%, 81.76%, and 74.64%, respectively.

Supplementary Materials: The following supporting information can be downloaded at: <https://www.mdpi.com/article/10.3390/ECP2023-14681/s1>, Figure S1: The Mass spectrometry peaks (m/z) of generated reaction intermediate during the photodegradation of MB dye with (a) 284 m/z, (b) 273 m/z, (c) 169 m/z, (d) 158 m/z, (e) 94 m/z; Figure S2: Identified transformation products and proposed photodegradation pathway of MB dye using ACPNS–TiO₂ nanocomposite catalyst.

Author Contributions: Conceptualization, K.S.; Methodology, K.S. and H.D.G.; validation, K.S. and H.D.G.; formal analysis K.S.; investigation, K.S.; data curation, K.S., H.D.G. and M.B.; writing—original draft, K.S.; writing—review and editing, K.S., H.D.G. and M.B.; supervision, H.D.G. All authors have read and agreed to the published version of the manuscript.

Funding: This research received no external funding.

Institutional Review Board Statement: Not applicable.

Informed Consent Statement: Not applicable.

Data Availability Statement: Not applicable.

Acknowledgments: The authors want to express their appreciation to the Japan International Cooperation Agency (JICA) and Egypt-Japan University of Science and Technology (E-JUST) for providing technical support.

Conflicts of Interest: The authors declare no conflict of interest.

References

1. Onen, N.; Elwardany, A.; Fujii, M. Biosorption of Congo Red dye from aqueous solutions using pristine biochar and ZnO biochar from green pea peels. *Chem. Eng. Res. Des.* **2023**, *189*, 636–651. [[CrossRef](#)]
2. Shindhal, T.; Rakholiya, P.; Varjani, S.; Pandey, A.; Ngo, H.H.; Guo, W.; Ng, H.Y.; Taherzadeh, M.J. A critical review on advances in the practices and perspectives for the treatment of dye industry wastewater. *Bioengineered* **2021**, *12*, 70–87. [[CrossRef](#)] [[PubMed](#)]
3. Safo, K.; Noby, H.; Matatoshi, M.; Naragino, H. Statistical optimization modeling of organic dye photodegradation process using slag nanocomposite. *Res. Chem. Intermed.* **2022**, *48*, 4183–4208. [[CrossRef](#)]
4. Shafique, M.; Mahr, M.S.; Yaseen, M.; Bhatti, H.N. CQD/TiO₂ nanocomposite photocatalyst for efficient visible light-driven purification of wastewater containing methyl orange dye. *Mater. Chem. Phys.* **2022**, *278*, 125583. [[CrossRef](#)]
5. Ren, L.; Zhou, W.; Sun, B.; Li, H.; Qiao, P.; Xu, Y.; Wu, J.; Lin, K.; Fu, H. Applied Catalysis B: Environmental Defects-engineering of magnetic γ -Fe₂O₃ ultrathin nanosheets/mesoporous black TiO₂ hollow sphere heterojunctions for efficient charge separation and the solar-driven photocatalytic mechanism of tetracycline deg. *Appl. Catal. B Environ.* **2019**, *240*, 319–328. [[CrossRef](#)]
6. Zhu, C.; Wang, X.; Huang, Q.; Huang, L.; Xie, J.; Qing, C.; Chen, T. Removal of gaseous carbon bisulfide using dielectric barrier discharge plasmas combined with TiO₂ coated attapulgite catalyst. *Chem. Eng. J.* **2013**, *225*, 567–573. [[CrossRef](#)]
7. Ao, W.; Qu, J.; Yu, H.; Liu, Y.; Liu, C.; Fu, J.; Dai, J.; Bi, X.; Yuan, Y.; Jin, Y. TiO₂/activated carbon synthesized by microwave-assisted heating for tetracycline photodegradation. *Environ. Res.* **2022**, *214*, 113837. [[CrossRef](#)] [[PubMed](#)]
8. Zeng, G.; You, H.; Du, M.; Zhang, Y.; Ding, Y.; Xu, C.; Liu, B.; Chen, B.; Pan, X. Enhancement of photocatalytic activity of TiO₂ by immobilization on activated carbon for degradation of aquatic naphthalene under sunlight irradiation. *Chem. Eng. J.* **2021**, *412*, 128498. [[CrossRef](#)]
9. Xu, W.; Jin, Y.; Ren, Y.; Li, J.; Wei, Z.; Ban, C.; Cai, H.; Chen, M. Synergy mechanism for TiO₂/activated carbon composite material: Photocatalytic degradation of methylene blue solution. *Can. J. Chem. Eng.* **2022**, *100*, 276–290. [[CrossRef](#)]
10. Safo, K.; Noby, H.; Matatoshi, M.; Naragino, H.; El-Shazly, A.H. Solvothermal Prepared Slag Nanocomposite as a Catalyst for Organic Dye Photodegradation. *Key Eng. Mater.* **2022**, *931*, 125–130. [[CrossRef](#)]
11. Gohoho, H.D.; Noby, H.; Hayashi, J.I.; El-shazly, A.H. Various acids functionalized polyaniline–peanut shell activated carbon composites for dye removal. *J. Mater. Cycles Waste Manag.* **2022**, *24*, 1508–1523. [[CrossRef](#)]
12. Rubangakene, N.O.; Elwardany, A.; Fujii, M.; Sekiguchi, H.; Shokry, H. Production of High Carbon Composite from Catalytic Pyrolysis of Pisum sativum Peels for Methylene Blue Dye Decolorization. In *Key Engineering Materials*; Trans Tech Publications Ltd.: Wollerau, Switzerland, 2022; Volume 935, pp. 171–177.
13. Tetteh, E.K.; Ezugbe, E.O.; Asante-Sackey, D.; Armah, E.K.; Rathilal, S. Response surface methodology: Photocatalytic degradation kinetics of basic blue 41 dye using activated carbon with TiO₂. *Molecules* **2021**, *26*, 1068. [[CrossRef](#)] [[PubMed](#)]
14. Safo, K.; Noby, H.; Mitsuhara, M.; Naragino, H.; El-shazly, A.H. H₂O₂ assisted steel slag nanocomposite for degradation of organic pollutant in an advanced oxidation process for suspension and Spin-Coated mode. *Environ. Nanotechnol. Monit. Manag.* **2023**, *20*, 100836. [[CrossRef](#)]

Disclaimer/Publisher's Note: The statements, opinions and data contained in all publications are solely those of the individual author(s) and contributor(s) and not of MDPI and/or the editor(s). MDPI and/or the editor(s) disclaim responsibility for any injury to people or property resulting from any ideas, methods, instructions or products referred to in the content.